PERGAMON

International Journal of Heat and Mass Transfer 45 (2002) 229–233

International Journal of HEAT and MASS TRANSFER

www.elsevier.com/locate/ijhmt

Technical Note

Momentum boundary layer and its influence on the convective heat transfer in porous media

D.-Y. Lee *, J.S. Jin, B.H. Kang

Thermal/Flow Control Research Center, Korea Institute of Science and Technology, P.O. Box 131, Cheongryang, Seoul 130-650, Republic of Korea

Received 27 September 2000; received in revised form 23 February 2001

Abstract

Convective heat transfer in a channel filled with a porous medium has been analyzed in this paper. The flow field is analyzed considering both the inertia and solid boundary effects and the thickness of the momentum boundary layer is found as a function of the Darcy and the Reynolds number. The two-equation model is applied for the heat transfer analysis and theoretical solutions are obtained for both fluid and solid phase temperature fields. The Nusselt number is obtained in terms of the relevant physical parameters, such as the Biot number for the internal heat exchange, the ratio of effective conductivities between the fluid and solid phases, and the thickness of the momentum boundary layer. The results indicate that the influence of the velocity profile is characterized within two regimes according to the two parameters, the Biot number and the conductivity ratio between the phases. The decrease in the heat transfer due to the momentum boundary layer is 15% at most within a practical range of the pertinent parameters.

Keywords: Porous media; Momentum boundary layer; Convective heat transfer; Nusselt number; Biot number; Conductivity ratio

1. Introduction

The utilization of porous inserts has proved to be very promising in heat transfer augmentation [1,2]. One of the important porous media characteristics is represented by an extensive contact surface between solid and fluid phases. The extensive contact surface enhances the internal heat exchange between the phases and consequently results in an increased thermal diffusivity. To account for the effect of the extensive contact surface in the analysis, it is required to utilize the two-equation model in which the two phases are treated separately and thermal communication between the phases across the contact surface is considered [3,4].

In the meanwhile, the increase in the pressure loss should also be considered to utilize the porous insertions into practical heat exchangers. From this point of view, a porous medium for this application is generally recommended to have a large porosity and permeability. In these situations, the velocity distribution and the resultant pressure loss are expected to be influenced much by the inertial force caused by the microstructure of porous media as well as the viscous drag by the impermeable wall containing the porous media [5,6]. Subsequently, the heat transfer is also expected to be influenced by these effects.

In the present study, the convective heat transfer in porous media is analyzed theoretically utilizing the two-equation model with the velocity distribution considering both the inertia and viscous effects. Based on the theoretical solution, the influence of the momentum boundary layer on the convective heat transfer in porous media is investigated.

2. Physical model and mathematical formulation

The problem under investigation is related to forced convective flow through a channel filled with a porous

* Corresponding author. Tel.: +82-2-958-5674; fax: +82-2-958-5689.

E-mail address: ldy@kist.re.kr (D.-Y. Lee).

0017-9310/02/$ - see front matter
PII: S0017-9310(01)00115-6

Nomenclature

a	surface area per unit volume (1/m)
Bi	Biot number defined in Eq. (11)
C_E	Ergun coefficient
Da	Darcy number defined in Eq. (5)
H	half of the channel height (m)
h_i	interstitial heat transfer coefficient (W/m^2 K)
h_w	wall heat transfer coefficient (W/m^2 K)
K	permeability (m^2)
k_{eff}	effective conductivity of the fluid (W/m K)
Nu	Nusselt number defined in Eq. (13)
q_w	heat flux at the wall (W/m^2)
Re_K	Reynolds number defined in Eq. (5)
T	temperature (K)
T_w	wall temperature (K)
U	fluid velocity (m/s)
U_c	fluid velocity at the channel center (m/s)

Greek symbols

δ	thickness of the momentum boundary layer nondimensionalized by H
ε	porosity
χ	nondimensional parameter defined in Eq. (11)

Subscripts

a	simplification of the velocity function
D	Darcian flow model
f	fluid
s	solid

medium. When the flow in the channel is fully developed, the momentum equation can be written as [7]:

$$\frac{d^2u}{d\eta^2} - \frac{1}{Da}(u-1) - \frac{Re_K}{Da}(u^2-1) = 0, \tag{1}$$

$$\frac{du}{d\eta} = 0 \quad \text{at } \eta = 0, \tag{2}$$

$$u = 0 \quad \text{at } \eta = 1, \tag{3}$$

in which the nondimensional variables and parameters are defined as:

$$u = \frac{U}{U_c}, \quad \eta = \frac{y}{H}, \tag{4}$$

$$Da = \frac{K}{\varepsilon H^2}, \quad Re_K = \frac{C_E U_c K^{1/2}}{\nu}. \tag{5}$$

When the heat transfer is fully developed, the energy equation for a constant heat flux boundary condition is obtained as [3]:

$$\chi \frac{\partial^2 \theta_f}{\partial \eta^2} + Bi(\theta_s - \theta_f) = \overline{u}, \tag{6}$$

$$\frac{\partial^2 \theta_s}{\partial \eta^2} - Bi(\theta_s - \theta_f) = 0, \tag{7}$$

$$\frac{\partial \theta_f}{\partial \eta} = \frac{\partial \theta_s}{\partial \eta} = 0 \quad \text{at } \eta = 0, \tag{8}$$

$$\theta_f = \theta_s = 0 \quad \text{at } \eta = 1, \tag{9}$$

in which the nondimensional variables and parameters are defined as:

$$\theta_f = \frac{k_{s,eff}(T_f - T_w)/H}{q_w},$$

$$\theta_s = \frac{k_{s,eff}(T_s - T_w)/H}{q_w}, \quad \overline{u} = \frac{u}{\langle u \rangle}, \tag{10}$$

$$Bi = \frac{h_i a H^2}{k_{s,eff}}, \quad \chi = \frac{k_{f,eff}}{k_{s,eff}}. \tag{11}$$

The wall heat transfer coefficient is defined by

$$h_w = \frac{q_w}{T_w - \langle u T_f \rangle / \langle u \rangle}, \tag{12}$$

where $\langle\,\rangle$ designates the average over the channel cross-section. The Nusselt number based on the channel hydraulic diameter and the effective fluid conductivity can be presented as

$$Nu = \frac{4 h_w H}{k_{f,eff}} = \frac{4}{\chi(-\langle u\theta_f \rangle / \langle u \rangle)}. \tag{13}$$

3. Momentum boundary layer

3.1. Simplification of the velocity equation

The analytical solution to the momentum equation, Eqs. (1)–(3) is obtained by Vafai and Kim [7] as:

$$u = 1 - \frac{C_1 + C_2}{C_1}\,\mathrm{sech}^2[C_3(\eta + C_4)], \tag{14}$$

$$C_1 = \frac{2}{3} Da^{-1} Re_K,$$

$$C_2 = Da^{-1} + \frac{4}{3} Da^{-1} Re_K, \tag{15}$$

$$C_3 = \frac{\sqrt{C_1 + C_2}}{2},$$

$$C_4 = -\frac{1}{C_3}\mathrm{sech}^{-1}\sqrt{\frac{C_1}{C_1 + C_2}} - 1.$$

The temperature distributions for the fluid and solid phases can be obtained by substituting Eq. (14) into Eq. (6) and integrating twice Eqs. (6) and (7) simultaneously. However, the analytical integration is nearly impossible due to the mathematical complexity of the velocity equation, Eq. (14)

In the meanwhile, it is found that the velocity distributions for various values of Da and Re_K are very similar to each other just within the momentum boundary layer even though the thickness of the boundary layer depends largely on the parameters. Based on this finding, a simple functional form is introduced to represent the velocity distribution approximately as follows:

$$u_a = 1 - \frac{\cosh(\eta/\delta)}{\cosh(1/\delta)}. \quad (16)$$

In this work, to approximate the general velocity distribution with Eq. (16), the parameter, δ, is so obtained as a function of Da and Re_K that the difference between the velocities evaluated from Eqs. (14) and (16) is minimized. Integrating Eqs. (14) and (16) over the channel cross-section yields the average velocities as:

$$\langle u \rangle = 1 - \frac{C_1 + C_2}{C_1 C_3}[\tanh(C_3(1 + C_4)) - \tanh(C_3 C_4)], \quad (17)$$

$$\langle u_a \rangle = 1 - \delta \tanh(1/\delta). \quad (18)$$

Using the least squares method with the assumption of $\delta \ll 1$, δ minimizing the velocity difference between Eqs. (17) and (18) is obtained as

$$\delta = \frac{C_1 + C_2}{C_1 C_3}[\tanh(C_3(1 + C_4)) - \tanh(C_3 C_4)]. \quad (19)$$

The comparison between Eqs. (17) and (19) reveals that the parameter, δ, represents exactly the displacement thickness due to the momentum boundary layer. In Fig. 1, the velocity profiles obtained by the exact solution, Eq. (14), are shown only near the wall by normalizing the distance from the wall by the parameter, δ. The values of the parameter, δ, are evaluated from Eq. (19) for each set of Da and Re_K and are arranged in a tablet in Fig. 1. With the new coordinate, the velocity profiles for various values of Da and Re_K are found to merge nearly into a single curve. The velocity profile using the approximating function, Eq. (16) is also plotted in Fig. 1. The approximating velocity profile is so well coincident with the exact velocity profiles that it is almost not distinguishable from others. The difference between the velocities obtained by Eqs. (14) and (16) is found to be 1.8% at most within the parameter range shown in Fig. 1, and to decrease with a decrease in Re_K.

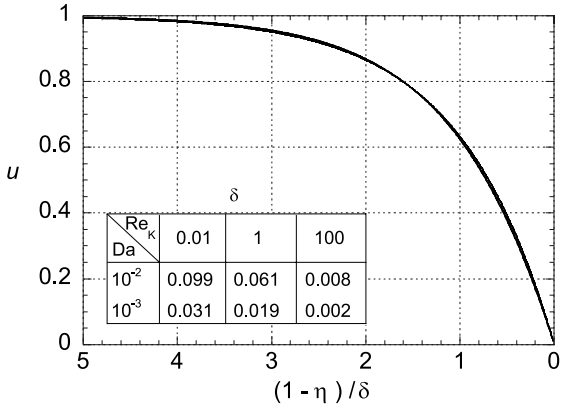

Fig. 1. Velocity distributions within momentum boundary layer.

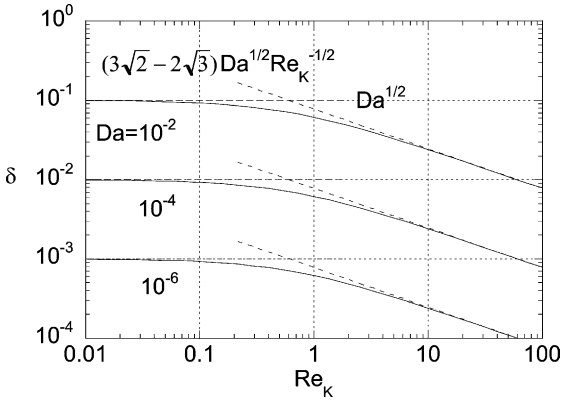

Fig. 2. Thickness of the momentum boundary layer.

3.2. Thickness of the momentum boundary layer

The variation of the thickness of the momentum boundary layer, δ, with respect to Da and Re_K is shown in Fig. 2. The asymptotic behavior is obtained by applying extreme values of Re_K into Eq. (19) and shown as dotted lines in this figure. An order of magnitude analysis is also made on the momentum equation Eq. (1), within the boundary layer to yield

$$\frac{1}{\delta^2} \sim \frac{1}{Da}(1 + Re_K). \quad (20)$$

This results in a similar dependency of the thickness of the momentum boundary layer to that shown in Fig. 2.

4. Heat transfer

4.1. Analytical solution to the two-equation model

As stated previously, it is nearly impossible to find the analytic solution to the temperature distributions using the two-equation model with the exact velocity profile due to the mathematical complexity of the exact velocity function, Eq. (14). In the meanwhile, the approximate velocity function, Eq. (16), has the same functional form as that of the exact velocity profile neglecting inertia force, and the corresponding solution to the two-equation model is already known [4]. Therefore,

the general solution to the two-equation model can be obtained by approximating the exact velocity profile considering both the inertia and viscous effects with Eq. (16) and applying this into the two-equation model. This yields:

$$\theta_f = \frac{1}{\langle u_a\rangle(1+\chi)}\left[\frac{1}{2}(\eta^2-1) - \frac{1}{\chi}\left(\frac{1}{\lambda^2}+\frac{\delta^2}{1-\lambda^2\delta^2}\right) \times\left(1-\frac{\cosh(\lambda\eta)}{\cosh(\lambda)}\right)+\delta^2\left(1+\frac{1}{\chi}\frac{1}{1-\lambda^2\delta^2}\right) \times\left(1-\frac{\cosh(\eta/\delta)}{\cosh(1/\delta)}\right)\right], \quad (21)$$

$$\theta_s = \frac{1}{\langle u_a\rangle(1+\chi)}\left[\frac{1}{2}(\eta^2-1) + \left(\frac{1}{\lambda^2}+\frac{\delta^2}{1-\lambda^2\delta^2}\right) \times\left(1-\frac{\cosh(\lambda\eta)}{\cosh(\lambda)}\right)+\delta^2\left(1-\frac{1}{1-\lambda^2\delta^2}\right) \times\left(1-\frac{\cosh(\eta/\delta)}{\cosh(1/\delta)}\right)\right], \quad (22)$$

where

$$\lambda = \sqrt{\frac{Bi(1+\chi)}{\chi}}. \quad (23)$$

Numerical integration of the energy equation applying the exact velocity profile, Eq. (14), for several sets of parameters reveals that the analytical solution, Eqs. (21) and (22), is accurate with the maximum difference of 1.5%.

The Nusselt number can be obtained by substituting Eq. (21) into Eq. (13).

4.2. Influence of the momentum boundary layer on the heat transfer

The Nusselt number is depicted in Fig. 3 as a function of *Bi* and δ for the two extreme values of χ, 10^{-6} and 10^{6}. The Nusselt number is normalized by the Nusselt number for the case without the momentum boundary layer, i.e., the case of the Darcian flow. Obviously, the normalized Nusselt number is shown to decrease with an increase in the thickness of the momentum boundary layer. When $\chi = 10^{-6}$, the normalized Nusselt number increases with the Biot number until $Bi = 0.1$ and decreases for further increases in *Bi* values. Meanwhile, when $\chi = 10^{6}$, the normalized Nusselt number is not influenced by the Biot number.

To show more clearly the influences of the parameters, *Bi* and χ, the normalized Nusselt number for $\delta = 0.1$ is depicted in Fig. 4 as a three-dimensional plot. This figure reveals the existence of two distinct regimes. Except the narrow boundary region between the two regimes, the normalized Nusselt number is shown to

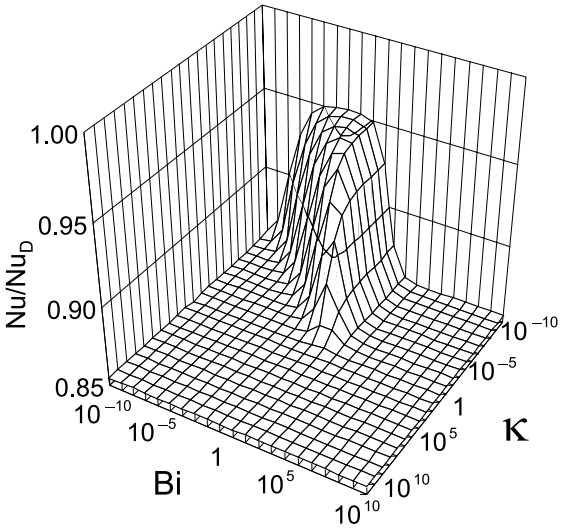

Fig. 4. Nusselt number reduction due to the momentum boundary layer ($\delta = 0.1$).

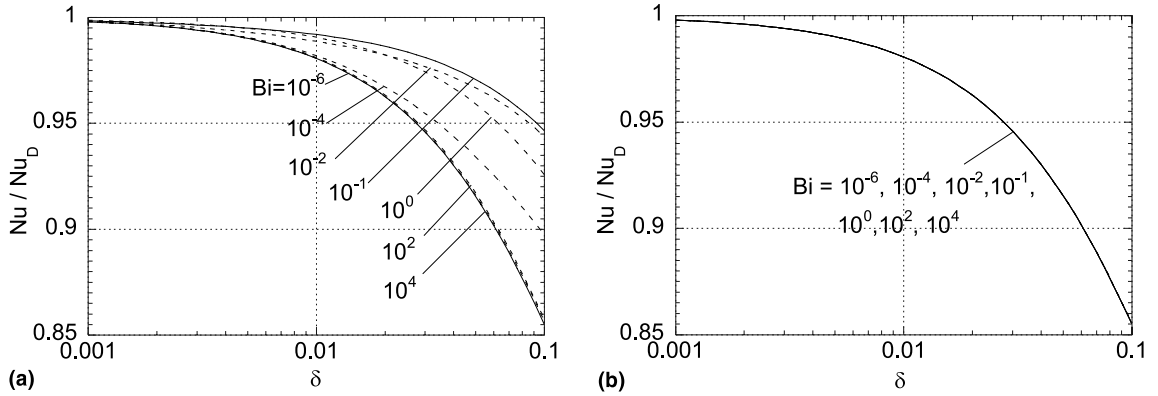

Fig. 3. *Nu* divided by Nu_D: (a) $\chi = 10^{-6}$; (b) $\chi = 10^{6}$.

have a constant value in each regime. From Fig. 4, the regime where the normalized Nusselt number is relatively large compared with other regime can be identified as $\chi \ll Bi \ll 1$.

Referring to Lee and Vafai [3], the energy equation, Eqs. (6) and (7) can be reduced to a simpler form by considering only the dominant factors in each regime as follows:

$$-Bi\theta_f \approx \bar{u} \quad \text{where } \chi \ll Bi \ll 1, \tag{24}$$

$$\chi \frac{\partial^2 \theta_f}{\partial \eta^2} \approx \bar{u} \quad \text{where } \chi \gg 1 \text{ or } \chi \gg Bi, \tag{25}$$

$$\frac{\partial^2 \theta_f}{\partial \eta^2} \approx \bar{u} \quad \text{where } \chi \ll 1 \text{ and } Bi \gg 1. \tag{26}$$

It can be found from the above equations that the fluid temperature profile is determined directly by the velocity profile in the regime where $\chi \ll Bi \ll 1$, and by the double integral in the other regimes. For this reason, the influence of the velocity profile on the heat transfer comes to be distinguished in each regime, which results in the two different normalized Nusselt numbers for the two distinct regimes.

5. Conclusion

The convective heat transfer in a channel filled with a porous medium is investigated based on the two-equation model with the velocity distribution considering both the inertia and solid boundary effects. A theoretical solution to the temperature field is obtained and the influence of the momentum boundary layer thickness on the heat transfer is investigated. In the regime where $\chi \ll Bi \ll 1$, the decrease in the wall heat transfer due to the momentum boundary layer is relatively small compared with the other regime. The decrease is found 15% at most within a practical range of the pertinent parameters.

Acknowledgements

This work was supported by a grant from the Critical Technology 21 Program of the Ministry of Science and Technology, Korea.

References

[1] J.C.Y. Koh, R.L. Stevens, Enhancement of cooling effectiveness by porous materials in coolant passage, J. Heat Transfer 97 (1975) 309–311.
[2] T.M. Kuzay, J.T. Collins, A.M. Khounsary, G. Morales, Enhanced heat transfer with metal-wool-filled tubes, Proc. ASME/JSME Thermal Eng. Conf. (1991) 145–151.
[3] D.-Y. Lee, K. Vafai, Analytical characterization and conceptual assessment of solid and fluid temperature differentials in porous media, Int. J. Heat Mass Transfer 42 (1999) 423–435.
[4] S.J. Kim, D. Kim, D.-Y. Lee, On the local thermal equilibrium in microchannel heat sinks, Int. J. Heat Mass Transfer 43 (2000) 1735–1748.
[5] G.S. Beavers, E.M. Sparrow, Non-Darcy flow through fibrous media, J. Appl. Mech. 36 (1969) 711–714.
[6] K. Vafai, C.L. Tien, Boundary and inertia effects on flow and heat transfer in porous media, Int. J. Heat Mass Transfer 24 (1981) 195–203.
[7] K. Vafai, S.J. Kim, Forced convection in a channel filled with a porous medium: an exact solution, J. Heat Transfer 111 (1989) 1103–1106.